Dissipative high-frequency envelope soliton modes in nonthermal plasmas

S. Sultana,[1,2,*] R. Schlickeiser,[2] I. S. Elkamash,[3,4] and I. Kourakis[4,5,†]

[1]*Department of Physics, Jahangirnagar University, Savar, Dhaka 1342, Bangladesh*

[2]*Fakultät für Physik und Astronomie, Ruhr-Universität Bochum, D-44780 Bochum, Germany*

[3]*Physics Department, Faculty of Science, Mansoura University, 35516 Mansoura, Egypt*

[4]*Centre for Plasma Physics, Department of Physics and Astronomy, Queen's University Belfast, Belfast BT7 1NN, Northern Ireland, United Kingdom*

[5]*Paris-Sorbonne University Abu Dhabi, P.O. Box 38044, Abu Dhabi, United Arab Emirates*

(Received 8 May 2018; published 14 September 2018)

The linear and nonlinear properties of modulated high-frequency (electron-acoustic) electrostatic wave packets are investigated via a fluid-dynamical approach. A three-component plasma is considered, composed of two types of electrons at different temperatures ("cold" and "hot" electrons) evolving against a cold stationary ion background. A weak dissipative effect is assumed, due to electron-neutral collisions. While the cold electrons are treated as an inertial fluid, the hot electrons are assumed to be in a non-Maxwellian state, described by a kappa (κ) type distribution. The linear characteristics of electron-acoustic waves are analyzed in detail, and a linear dispersion relation is obtained. Weakly damped electrostatic waves are shown to propagate above a wave number k threshold, whose value is related to dissipation (and reduces to zero in its absence). Long-wavelength values (i.e., for k below that threshold) are heavily damped and no propagation occurs. The nonlinear dynamics (modulational self-interaction) of wave packets in the propagating region is modeled via a dissipative nonlinear Schrödinger type equation, derived via a multiscale perturbation technique for the wave envelope, which includes a dissipative term associated with the finite imaginary part of the nonlinearity term. The dynamical and structural characteristics (speed, amplitude, width) of dissipative localized modes representing the amplitude of modulated electron-acoustic wave packets in a collisional plasma are thus investigated for various values of relevant plasma (configuration) parameters, namely the superthermality index κ, the cold-to-hot electron density ratio, and collisionality (strength). Our analytical predictions are tested by computer simulations. A quasilinear perturbation method for near-integrable systems leads to a theoretical prediction for the wave amplitude decay, which is shown to match our numerical result. The results presented in this paper should be useful in understanding the dynamics of localized electrostatic disturbances in space plasmas, and also in laboratory plasmas, where the combined effect(s) of excess energetic (suprathermal) electrons and (weak) electron-neutral collisions may be relevant.

DOI: 10.1103/PhysRevE.98.033207

I. INTRODUCTION

Localized structures, in the form of electrostatic solitary waves (ESWs) are known to propagate in plasmas thanks to a delicate balance between nonlinearity and dispersive effects [1]. Although ESWs are often modeled as *solitons*, i.e., steady state solutions of integrable nonlinear partial differential equations (PDEs), they may be subject to external perturbations, such as wave-wave interactions, forcing, or dissipation (damping)—of importance here—during propagation; it is known that, for external perturbations which are not "too" strong, solitons may adapt their propagation characteristics (amplitude, width, speed) and still propagate for long distances, eventually decaying in time [2].

Dissipative solitary waves (or *dissipative solitons*) are known in plasma physics [3–10] and also in nonlinear optics [11–16]. In plasmas, dissipation may arise due to collisions among different plasma constituents (e.g., electron-neutral collisions [17], ion-neutral collisions [18], dust-ion collisions [18], dust-neutral collisions [17], due to nonlinear Landau damping [19], or finally due to kinematic fluid viscosity [20]).

Real plasmas, both in space and in laboratory, are most often *not* in thermodynamic equilibrium; instead, they are characterized by energetic particles, which are accelerated via different mechanisms. This is reflected in an excess population in the fast (superthermal) particle velocity distribution component, which thus deviates from the (thermal) Maxwellian distribution function and rather acquires a long-tailed power law dependence, as observed in space [21–24]. This behavior is successfully described via the κ (kappa) nonthermal distribution function [24–27], as a plethora of *in situ* observations have shown, both in space plasmas [28–30] and in the laboratory [31–33].

Nonlinear wave propagation in plasmas is dynamically affected by accelerated (superthermal) particles (electrons or/and ions), as shown in a number of theoretical investigations, modeling solitary waves [34–36], shock waves [37,38], double layers [39], and modulated wave packets [38,40].

Modulational processes involved in the dynamics of electrostatic wave packets are known to be modeled by the cubic nonlinear Schrödinger equation (NLSE) [38,40,41]. In

*ssultana@juniv.edu

†IoannisKourakisSci@gmail.com

an alternative formulation, in optics, electromagnetic wave packets are modeled by a Ginzburg-Landau type equation (GLE) [3–6], in the presence of gain and loss terms, i.e., due to dissipation. This mainly affects nonlinear phenomena, such as modulational instability (MI), a well-known generic mechanism for energy localization in nonlinear and dispersive media [1]. Importantly, envelope solitons, modeled by either NLSE or GLE theories, are used in telecommunications [42], to model signal transmission via pulses propagating in optical fibers, due to their remarkable stability properties. In a real-life dissipative system, an external source of energy (amplifier, amplitude modulator) [43] is added to sustain the original information over a very long distance, e.g., in fiber optics. The external energy thus balances dissipation, and the initial solitary pulse maintains its stability while propagating through a balance of gain and loss mechanisms.

Decades ago, Nicholson [3] used the NLSE paradigm to model high-frequency electrostatic plasma oscillations in the simultaneous presence of collisional and Landau damping by adopting a kinetic (statistical) approach, arguing that Landau damping results in a soliton pulse which is shorter (of smaller amplitude) and wider (in spatial extension) due to decay, while collisional damping may result in narrower and smaller solitons, with constant speed [3]. An *ad hoc* NLSE model with complex coefficients was adopted in Ref. [4] to describe the combined action of growth and damping processes in plasmas. A localized soliton-like steady state was proposed [4], and the characteristic soliton parameters of the soliton (amplitude, width) were found analytically, assuming that the pulse's shape remains unchanged.

The investigation at hand focuses on electron-acoustic waves (EAWs) [44–50], i.e., a propagating electrostatic mode sustained thanks to inertia being provided by a "cold" electron fluid, while the restoring force is provided by the thermal pressure of a "hot" electron fluid, both evolving against a neutralizing ion background [44–50]. The hot electron population is characterized by an excess in the superthermal region of its (non-Maxwellian) particle distribution, which is effectively modeled by a kappa (κ) type distribution function. Interestingly enough, these conditions are satisfied in Saturn's magnetosphere [51], where a coexistence of electron populations (at distinct temperatures) is observed, with κ index varying from $\kappa \simeq 2$ to 4 in a wide region. Nonlinear electron-acoustic (EA) structures have been studied via different theoretical approaches in the recent past [10,40,52–54].

From a methodological point of view, we have applied a multiple scale technique to derive an evolution equation for the electrostatic potential ϕ. We have thus been led to a modified version of the well-known nonlinear Schrödinger (NLS) equation, the novelty lying in the fact that the nonlinearity coefficient is now complex-valued, in account of dissipation (due to an *ad hoc* damping term adopted in the dynamics to model weak plasma collisionality). Building up on earlier knowhow [7,10,38,40,41], we aim at modeling the dynamical evolution of modulated amplitude electron-acoustic wave packets, and investigating their dynamical dependence on different plasma composition parameters and mechanisms: dissipation, superthermality, composition.

The layout of this paper is as follows. A fluid model for high-frequency electrostatic wave packets is presented in Sec. II. A linear dispersion relation is derived and the linear properties of EAWs are analyzed in Sec. III. A nonlinear analysis is carried out and an evolution equation is derived for the wave packet amplitude (envelope) and the role of damping is then discussed in Sec. IV. A parametric investigation is presented, based on a critical comparison of analytical and numerical (simulation) results, in Sec. V. Finally, our results are summarized in the concluding Sec. VI.

II. FLUID MODEL

We consider a three-component unmagnetized collisional plasma consisting of cold (inertial) electron, hot (inertialess) electrons (characterized by a nonthermal κ distribution), and stationary (positively charged) ions.

We focus on the dynamical motion of the cold electron population, considered to be dominant in our scale of interest, by assuming that the wave's phase speed is far smaller than the hot electrons' thermal speed, and much greater than both ions' and cold electrons' thermal speed, i.e., $v_{th,i},\ v_{th,c} \ll v_{ph} \ll v_{th,h}$ (the indices i, c, and h denote the ions, cold electrons, and hot electrons, respectively). Working in a one-dimensional (1D) geometry, the "cold" electron component is described by the fluid-dynamical equations

$$\frac{\partial n_c}{\partial t} + \frac{\partial (n_c u_c)}{\partial x} = 0, \tag{1}$$

$$\frac{\partial u_c}{\partial t} + u_c \frac{\partial u_c}{\partial x} = \frac{e}{m_e}\frac{\partial \Phi}{\partial x} - \nu_c u_c, \tag{2}$$

$$\frac{\partial^2 \Phi}{\partial x^2} = 4\pi e[n_c + n_h - Z_i n_{i0}]. \tag{3}$$

The "hot" electrons are assumed to be in a non-Maxwellian state, modeled by the kappa (κ) distribution function [21,25,55]:

$$n_h = n_{h0}\left[1 - \frac{e\Phi}{k_B T_h(\kappa - 3/2)}\right]^{-\kappa+1/2}, \tag{4}$$

where the spectral index κ is a real parameter which measures the deviation from the Maxwell-Boltzmann equilibrium state: note that smaller values of κ imply stronger deviation (nonthermal behavior), while the appropriate expression(s)' Maxwellian state is recovered in the infinite-κ limit [25].

We may now normalize Eqs. (1)–(4), for tractability and analytical convenience. This is achieved by adopting appropriate scales, to be defined below. We thus obtain the rescaled (dimensionless) equations

$$\frac{\partial n}{\partial t} + \frac{\partial (nu)}{\partial x} = 0, \tag{5}$$

$$\frac{\partial u}{\partial t} + u\frac{\partial u}{\partial x} = \frac{\partial \phi}{\partial x} - \nu u, \tag{6}$$

$$\frac{\partial^2 \phi}{\partial x^2} \simeq \beta(n-1) + c_1\phi + c_2\phi^2 + c_3\phi^3, \tag{7}$$

where the cold electron fluid number density n_c and velocity u_c are normalized by the equilibrium number density n_{c0} and the characteristic (hot) electron thermal speed $v_0 = (T_h/m_e)^{1/2}$, respectively, while the electrostatic potential Φ is scaled by $\Phi_0 = T_h/e$. The space x and time t variables

are scaled by the hot electron screening length $\lambda_{Dh} = (T_h/4\pi n_{h0}e^2)^{1/2}$ and by the hot electron plasma period (inverse frequency) $\omega_{ph}^{-1} = (4\pi n_{h0}e^2/m_e)^{-1/2}$, respectively. The normalized collisionality parameter now reads $\nu = \nu_c/\omega_{ph}$. We have defined the cold-to-hot electron density ratio as $\beta = n_{c0}/n_{h0}$. Note that the right-hand side of Eq. (7) was expanded to a McLaurin series near equilibrium; hence the suprathermal electron feature (manifested via κ) is now incorporated in the coefficients c_1, c_2, and c_3, respectively given by $c_1 = \frac{\kappa-1/2}{\kappa-3/2}$, $c_2 = \frac{c_1(\kappa+1/2)}{2(\kappa-3/2)}$, and $c_3 = \frac{c_2(\kappa+3/2)}{3(\kappa-3/2)}$. Here, T_c (T_h) denotes the temperature of the cold (hot) electron component, in energy units (the Boltzmann constant was omitted where obvious).

It should be stressed, for rigor, that electron-acoustic wave propagation is possible provided that the phase speed (value) lies between the thermal speed of the hot and cold electron populations, so that the waves do not resonate with either particle component (thermal speeds), thus avoiding resonant damping. In general electron-acoustic waves suffer strong Landau damping generated by the hot electron population; practically speaking, they do survive for a temperature ratio $T_h/T_c \gg 10$ and for a density ratio $0.25 \leqslant n_{c0}/n_{h0} \leqslant 4$ [40,46,56], where the subscript h (c) obviously denotes the hot (cold, respectively) electrons. In other words, the hot electron population needs to be less than 25% that of cold electron population, so as to render propagation of EAWs possible in the plasma. It has also been pointed out in Ref. [56] (see Figs. 3–5 therein, as well as the accompanying discussion) that the region in the relevant parameter space (carrier wave number, spectral index κ, hot/cold electron population density ratio) needed to ensure weak damping of EAWs becomes smaller, if one consider lower values of the ratio T_h/T_c and/or lower κ (i.e., stronger deviation from the Maxwellian equilibrium state).

III. LINEAR ANALYSIS

To model linear waves, we proceed by considering harmonic perturbations of the dependent (state) variables as $e^{i(kx-\omega t)}$, where ω and k denote the wave frequency and wave number, respectively. A dispersion relation relating ω and k is thus obtained, upon linearizing the dimensionless system of evolution equations (5)–(7), in the form

$$\omega(\omega + i\nu) = \frac{\beta k^2}{k^2 + c_1}. \tag{8}$$

Assuming that the condition

$$\frac{\beta k^2}{k^2 + c_1} - \frac{\nu^2}{4} > 0$$

is satisfied, we may separate real and imaginary parts to obtain

$$\omega = -i\frac{\nu}{2} + \sqrt{\frac{\beta k^2}{k^2 + c_1} - \frac{\nu^2}{4}}. \tag{9}$$

The real part of the frequency ω_r is a function of the plasma intrinsic configuration parameters (namely, superthermality via κ, electron concentration ratio via β, and collisionality via ν), while the imaginary part ω_i is associated with collisionality, depending only on the parameter ν. The above condition implies that the wave number exceeds a certain threshold $k_c = [c_1\nu^2/(4\beta - \nu^2)]^{1/2}$ ($\simeq \sqrt{c_1/\beta}\,\nu/2$, for $\nu \ll \sqrt{\beta}$).

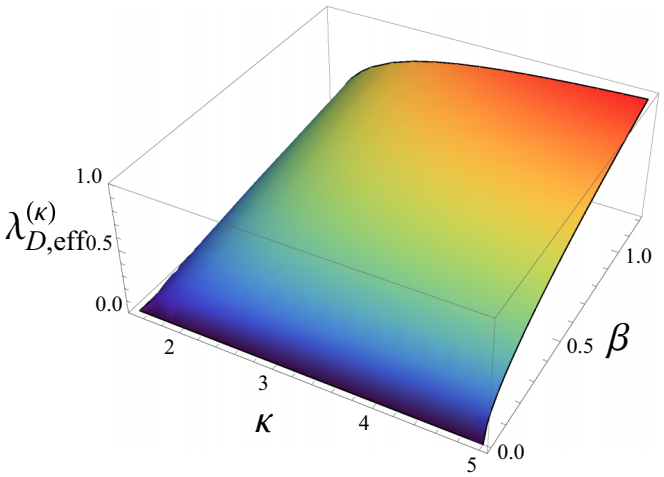

FIG. 1. The variation of the κ-dependent Debye screening length $\lambda_{D,\mathrm{eff}}^{(\kappa)}$, from (10), is depicted versus the hot electron spectral (superthermality) index κ and the cold-to-hot electron number density ratio β.

We conclude that wave packets with short-wavelength value, i.e., for $k > k_c$, will propagate, while the carrier wave will experience amplitude attenuation (decay) as

$$e^{i(kx-\omega t)} = e^{-i\nu t/2}e^{i(kx-\omega_r t)}.$$

The smaller the value of ν, the longer the propagation distance will be.

On the other hand, for lower wave number $k < k_c$, the wave will be strongly damped and aperiodic, since $\omega_r = 0$ and $\omega_i = -\frac{\nu}{2} \pm (\frac{\nu^2}{4} - \frac{\beta k^2}{k^2+c_1})^{1/2}$ (both solutions are negative; the minus sign will be dominant in this case).

As a matter of fact, the dispersion relation (9) suggests that $\omega_r \simeq (\frac{\beta}{c_1})^{1/2}k$, for $k \ll c_1^{1/2}$ and $\nu \simeq 0$, suggesting that the phase speed is $v_{ph} \approx (\frac{\beta}{c_1})^{1/2}$ in this case. This is the true phase speed of EAWs in this kind of plasma, a result which is in agreement with Ref. [56]. The same (dimensionless) quantity may be interpreted as the κ-dependent Debye screening length:

$$\lambda_{D,\mathrm{eff}}^{(\kappa)} = \left(\frac{\beta}{c_1}\right)^{1/2} = \frac{\kappa - \frac{3}{2}}{\kappa - \frac{1}{2}}\frac{n_{c0}}{n_{h0}}. \tag{10}$$

We note that the κ-dependent Debye screening length, say $\lambda_{D,\mathrm{eff}}^{(\kappa)}$, reduces to zero in either of the limits $\kappa \to 3/2$ or $\beta \to 0$ (see in Fig. 1) as physically expected [65], from previous works [40,56]. Finally, a Taylor series near the wave number threshold $k_c = \frac{\sqrt{c_1}\nu}{\sqrt{4\beta-\nu^2}}$, discussed above, yields

$$\omega_r \simeq \frac{\nu(4\beta - \nu^2)^{3/2}}{8\beta\sqrt{c_1}}(k - k_c) \approx \frac{\sqrt{\beta}}{\sqrt{c_1}}\nu\left(k - \frac{\sqrt{c_1}\nu}{2\sqrt{\beta}}\right). \tag{11}$$

The threshold takes small values, e.g., $k_c \simeq 0.488$ for representative values $\kappa = 3$, $\beta = 0.5$, and $\nu = 0.5$; see Fig. 2. The threshold increases (extending the "forbidden," overdamped region to larger k) for stronger dissipation (i.e., for larger ν).

In Fig. 3, we depict the threshold wave number k_c against the collision frequency ν for different cold-to-hot electron

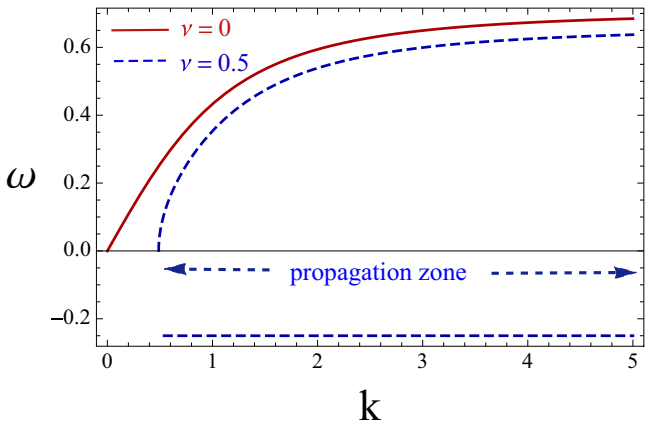

FIG. 2. Dispersion relation: The wave frequency ω is depicted versus the wave number k. Here, we have considered a strong superthermality index value $\kappa = 3$, along with a cold-to-hot electron number density ratio $\beta = 0.5$. The positive upper part denotes the real part of the frequency, ω_r, while the constant negative part at the bottom of the graph denotes the imaginary part ω_i.

population ratio β and also for different superthermality parameter κ. Note that the threshold practically varies linearly (since $\nu \ll \sqrt{\beta}$ in all realistic cases), i.e., $k_c \simeq \sqrt{\frac{c_1}{\beta}}\frac{\nu}{2}$, as seen in the plots. The wave number threshold is actually lower for a higher cold electron concentration in the plasma, as seen in Fig. 3(a). On the other hand, k_c is lower in a Maxwellian plasma (large κ) than in a nonthermal plasma (for low κ values), as depicted in Fig. 3(b). It is seen in Fig. 4 that the real part of the wave frequency ω_r (in the region $k > k_c$) increases as either β or ν increase.

As discussed in the introduction, electron-acoustic waves are sensitive to Landau damping (though this is inevitably neglected in a fluid description, like in our case), so these can survive only for specific values of the cold-to-hot electron number density [46,47,53]. We shall therefore consider appropriate values of the cold-to-hot electron density ratio β in the following.

The wave packet's envelope propagates at the group velocity $v_g = d\omega/dk = d\omega_r/dk$ which, based on Eq. (8), is given by

$$v_g = \frac{\beta k c_1}{(k^2 + c_1)^2}\frac{1}{\omega_r}, \tag{12}$$

which is a real (positive) quantity for $k > k_c$. The reality of the group velocity confirms the fact that electron-acoustic (EA) wave packets will not suffer any dispersive loss during their propagation in the plasma.

IV. NONLINEAR ANALYSIS

We proceed by adopting a multiple (space and time) scales technique, following the methodology described in Refs. [40,41,57]. The method is only briefly summarized here, since details on the tedious procedure are provided in Appendix A. The algebraic procedure amounts to considering excitations off-equilibrium, expressed by a series of the form $\phi \simeq \epsilon\phi_1^{(1)} e^{i\theta} + \epsilon^2(\phi_0^{(2)} + \phi_1^{(2)} e^{i\theta} + \phi_2^{(2)} e^{2i\theta} + \cdots$,

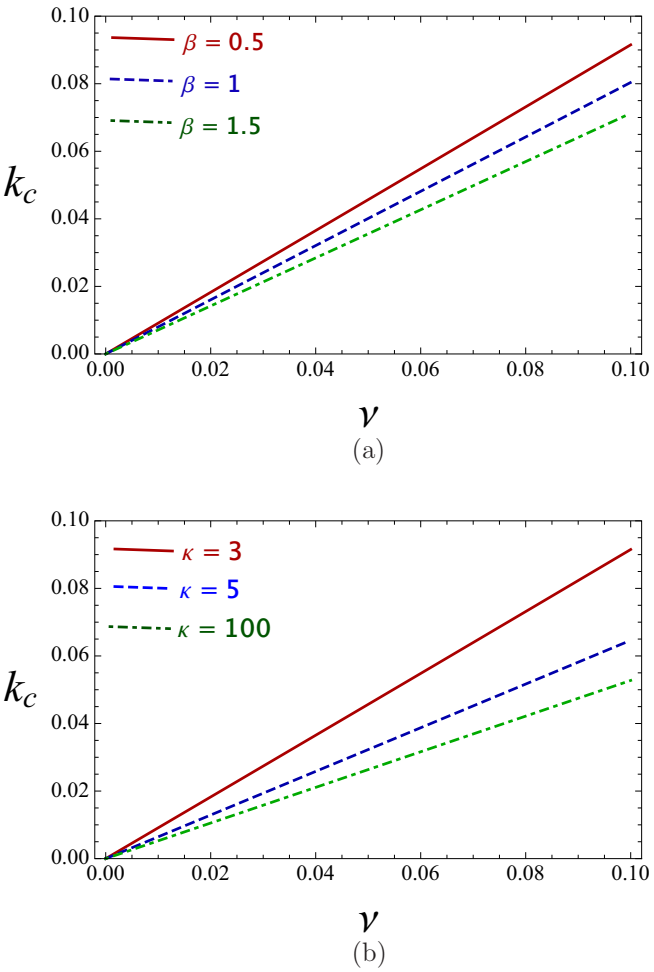

FIG. 3. The wave number threshold k_c is shown versus the collisional parameter ν: (a) for different cold-to-hot electron population ratio β (for $\kappa = 3$, here), and (b) for different κ (with $\beta = 0.5$).

where $\theta = kx - \omega t$ is the fundamental (leading harmonic) phase and $\epsilon \ll 1$ is a small (real) parameter. (Analogous expressions are obtained for the remaining state variables, i.e., the cold electron density n_c and fluid speed u_c, in our model.) Details on the tedious algebraic procedure, as well as the set of expressions obtained for the various coefficients associated with second-order zeroth, first, and second harmonics, are described in Appendix A.

A. Nonintegrable NLS equation for dissipative envelope soliton modes

The condition for annihilation of secular terms in third order in ϵ ($n = 3$) results in a closed PDE for the first harmonic ($l = 1$), in terms of the leading harmonic amplitude $\phi_1^{(1)}$. This equation takes the form of a cubic nonlinear Schrödinger equation in the form

$$i\left(\frac{\partial\phi_1^{(1)}}{\partial T_2} + v_g\frac{\partial\phi_1^{(1)}}{\partial X_2}\right) + P\frac{\partial^2\phi_1^{(1)}}{\partial X_1^2} + Q\left|\phi_1^{(1)}\right|^2\phi_1^{(1)} = 0, \tag{13}$$

where $T_2 = \epsilon^2 t$, $X_2 = \epsilon^2 x$, and $X_1 = \epsilon x$ are slow time and space variables. Now, applying the Galilean coordinate

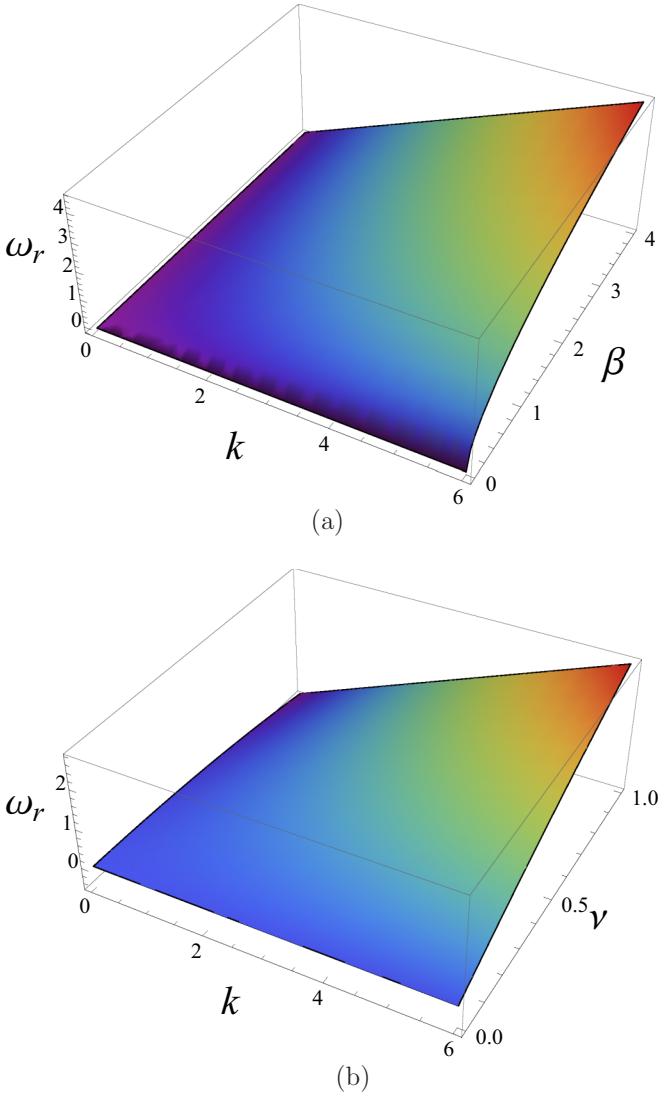

FIG. 4. The variation of the wave frequency ω_r (real part), as given in Eq. (11), is shown (a) versus the wave number k and the cold-to-hot electron number density ratio β, for $\kappa = 3$ and $\nu = 0.5$, and (b) versus the wave number k and the collisional parameter ν, for $\kappa = 3$ and $\beta = 0.5$.

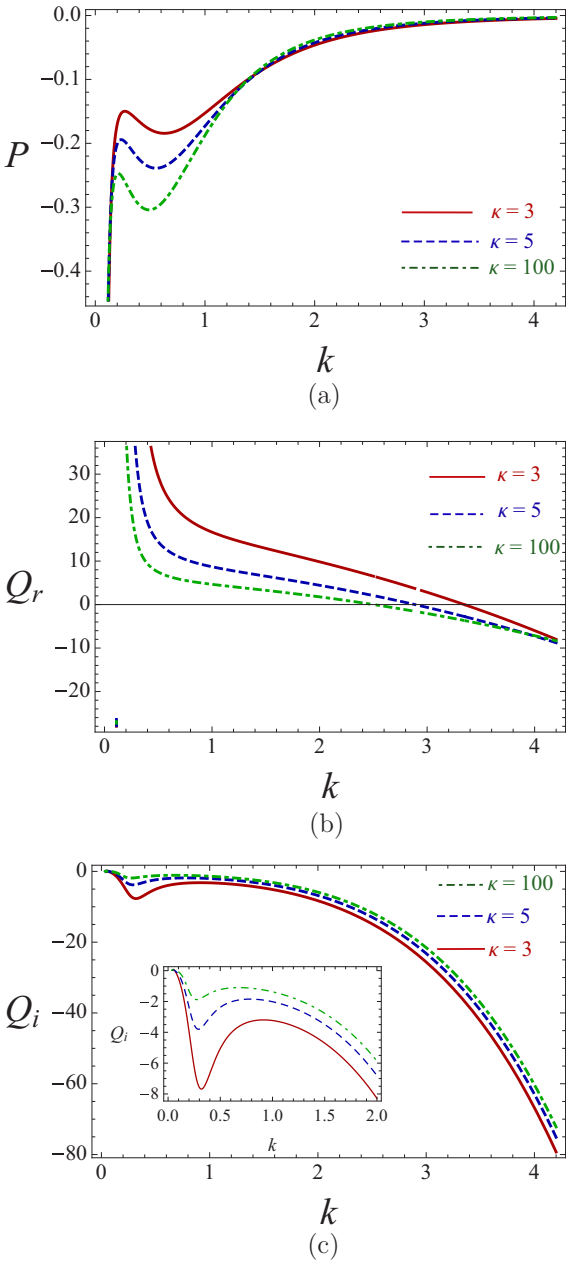

FIG. 5. We depict the effect of superthermality (via κ) on (a) the dispersive term P, (b) the real part of nonlinear term Q_r, and (c) the imaginary part of nonlinear term Q_i, versus the wave number k for $\beta = 0.5$, $\nu = 0.05$. The inset figures show a zoom-in view of regions of interest.

transformation $\zeta = x - v_g t$, $\tau = t$, one finds the standard form of the NLS equation:

$$i\frac{\partial\psi}{\partial\tau} + P\frac{\partial^2\psi}{\partial\zeta^2} + Q|\psi|^2\psi = 0, \tag{14}$$

where ψ denotes the electric potential correction $\phi_1^{(1)}$. The group velocity dispersion coefficient P $(= \frac{1}{2}\frac{d^2\omega}{dk^2})$ is a real-valued parameter, given by the expression (B1) in Appendix B. The nonlinearity coefficient Q is given by a lengthy expression, also provided in Appendix B; see Eq. (B2). The approximate expressions of the dispersion term P and the nonlinear term Q for small ν are provided in Appendix C.

A very important comment must be made at this stage. Although Eq. (14) is reminiscent in structure of the standard form of the NLS equation (see, e.g., in Refs. [1,41]), it is *not* identical to the "traditional" (integrable, actually) form of the NLSE, which is characterized by real dispersion (P) and nonlinearity (Q) coefficients. On the contrary, although P is real, $Q = Q_r + i\,Q_i$ is actually a complex quantity in our case. Closed analytical expressions for the real part Q_r and the imaginary part Q_i are provided in Appendix B. It is straightforward to verify [either analytically or numerically; cf. Fig. 5(c)] that Q_i tends to zero, for vanishing ν, as expected.

The real-valued P in combination with the complex-valued Q suggest a decaying electrostatic mode; i.e., the amplitude of the wave is expected to decay with time. The dispersion

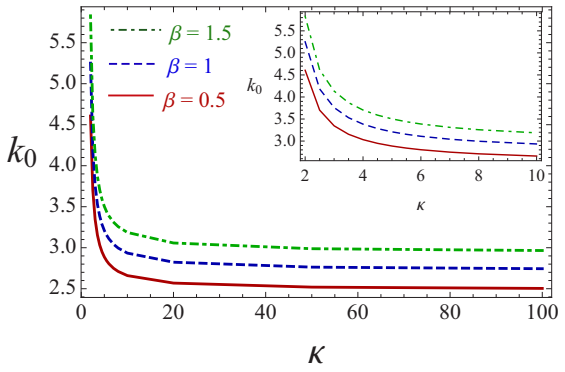

FIG. 6. Variation of the wave number threshold k_0 [in which $Q_r(k_0) = 0$] versus the superthermality index κ for different values of cold-to-hot electron number density ratio β, where $\nu = 0.05$. The inset figures show a zoom-in view of regions of interest.

term P will seek to balance the nonlinear term, i.e., the real part of the nonlinear coefficient Q_r. However, the nonlinear Schrödinger equation (14) does not have the dispersive gain term, i.e., does not have an imaginary part in the dispersive coefficient to balance Q_i. As a consequence, no source exists to balance the nonlinear loss term, i.e., with the imaginary part of the nonlinear coefficients Q_i, and thus the coefficient Q_i will lead to nonlinear decay of the wave envelope.

The effect of nonthermality (via κ) on the coefficients P, Q_r, and also Q_i in the presence of damping is explored in Fig. 5. It is evident that the dispersion term P and the imaginary part of nonlinearity coefficient Q_i are negative for any value of wave number k. On the other hand, the real part of nonlinearity coefficient Q_r is positive for low k (long wavelength), but becomes negative for higher values of wave number k (short wavelength). The value of the wave number where Q_r vanishes, i.e., the root k_0 [viz., $Q_r(k_0) = 0$] is obviously a function of β and κ, to be obtained numerically. The value of k_0 decreases with lower κ, down from a maximum value $k_0 \simeq 2.5$, for very large κ (i.e., in the Maxwellian limit), all the way down to $k_0 \simeq 3.35$ for $\kappa \simeq 3$ (anti-Maxwellian limit). This behavior is visible in Figs. 5(b) and 6. Interestingly, the threshold tends to infinity as κ approaches its lower bound 3/2; hence Q_r is positive for any wave number, for very small κ (near 1.5). Practically speaking, the focusing (bright soliton) condition $PQ_r > 0$ will never be realized for strongly non-Maxwellian plasmas therefore, rendering bright-type excitations (bright soliton, breathers, rogue wave structures) unstable, for any realistic (except infinitesimally short) carrier wavelength values, in the very low κ ($\leqslant 2$, roughly) regime. One thus draws the general conclusion that superthermality invalidates bright electroacoustic envelope solitons, for ultralow values of κ (these are actually not frequent in space observations, which are mostly consistent with values in the region $2 < \kappa < 6$).

It is known that the *integrable* NLSE, here recovered from (14) upon setting $Q_i = Q_i(\nu = 0) = 0$, possesses bright-type envelope soliton modes in the so-called focusing regime, i.e., when $PQ_r > 0$ (in our notation, here). In the opposite case, where $PQ_r < 0$, dark-type envelope soliton modes are obtained. Upon simple inspection of Fig. 5, it is obvious that the focusing regime is realized in our case for high-wave-number values, i.e., for carrier wave number above (the root of Q_r) k_0. We shall now proceed by considering this (focusing) region only.

B. Canonical form of the NLSE

We now introduce new rescaled coordinates for the time and space variables, as well as for the wave amplitude, as

$$T = |Q_r|\psi_0^2\,\tau, \quad \xi = |Q_r/2P|^{1/2}\,\psi_0\,\zeta, \quad \psi = \psi/\psi_0, \quad (15)$$

where ψ_0 represents a characteristic (electrostatic potential) wave amplitude scale (left arbitrary at this stage). Introducing (15) into Eq. (14) and separating the real and imaginary parts, one finds a reduced form of the NLSE as

$$i\frac{\partial\psi}{\partial T} + \frac{\alpha_1}{2}\frac{\partial^2\psi}{\partial\xi^2} + \alpha_2|\psi|^2\psi = -i\alpha_3 D|\psi|^2\psi, \quad (16)$$

where $\alpha_1 = P/|P| = \pm 1$, $\alpha_2 = Q_r/|Q_r| = \pm 1$, and $\alpha_3 = Q_i/|Q_r| = \pm 1$ denote the sign(s) of the respective coefficients. Note that (16) is valid in general, obtained upon imposing the scaling (15) on Eq. (14) above. In our case, $\alpha_1 = \alpha_3 = -1$, while $\alpha_2 = +1$ in the "defocusing" (modulationally stable) region $k < k_0$, or $\alpha_2 = -1$ in the "focusing" (modulationally unstable) region $k > k_0$. (These signs can be inferred upon simple inspection from Fig. 5.) Note that $D = |Q_i/Q_r|$ is the (absolute value of the) ratio of the imaginary to real nonlinearity coefficients, in fact a positive definite quantity.

Combining the above considerations, and henceforth limiting our attention to the "focusing" (modulationally unstable) region $k > k_0$ (i.e., for $P\,Q_r > 0$), we obtain from (16) the following variant of the canonical form of the NLSE:

$$i\frac{\partial\psi}{\partial T} - \frac{1}{2}\frac{\partial^2\psi}{\partial\xi^2} - |\psi|^2\psi = iD|\psi|^2\psi = f[\psi], \quad (17)$$

where we have formally defined the right-hand side via the action of the operator $f[\psi] = iD|\psi|^2\psi$.

We note, for rigor, that the scaling (15) adopted above introduces space and time scales which are actually functions of the wave number k (via P and Q_r), alongside plasma parameters (κ, β). The reduction of Eq. (14) to the latter "canonical" form (17), carried out here, will be important as an algebraic procedure, not only to pinpoint the effect of dissipation, but also to discuss, e.g., relevant mathematical properties of Eq. (17) as a nearly integrable dynamical system and to serve as basis for numerical simulation (see next section). However, the resulting equation cannot be used for a parametric investigation anymore, since relevant plasma (configuration) parameters are now "hidden" in the scales.

In the case $f[\psi] = 0$ (only), the nonlinear Schrödinger equation (17) possesses an infinite number of conserved quantities (integrals). Following Ref. [58], upon formally setting $q = \psi$ and $R[q] = f[\psi]$ therein, we define the energy and momentum integrals [58–60]

$$E = \int_{-\infty}^{\infty} |\psi|^2 d\xi \quad (18)$$

and

$$M = \frac{1}{2}\int_{-\infty}^{\infty} (\psi\psi_\xi^* - \psi^*\psi_\xi)d\xi, \quad (19)$$

respectively, where ψ_ξ represents the derivative of ψ with respect to ξ.

It is well known that plane wave solutions become unstable [1] for $PQ_r > 0$ (in the case $f = 0$). Bright type envelope modes [41,57,61–63] also occur under the same condition. The bright soliton solution [59,64] (for $D = 0$) has the form

$$\psi = \rho\,\mathrm{sech}[\rho(\xi - v\,T)]\exp[i\{v\,\xi + (\rho^2 - v^2)T/2\}], \quad (20)$$

which represents an envelope with constant amplitude ρ and velocity v. By combining Eqs. (18), (19), and (20), we obtain the soliton energy and momentum as

$$E = 2\rho, \qquad M = -2i\rho v, \quad (21)$$

respectively.

As we now have to deal with a dissipative dynamical system, the wave may not have a constant amplitude and/or velocity. Assuming a state off (but not far from) the steady state solution of the integrable problem, we may allow the amplitude ρ and the velocity v of the wave to vary in time T and space ξ, assuming the expression (20) to be still valid in the dissipative ("near-integrable") case. We now consider the complete NLSE (17), to trace the evolution of the wave amplitude ρ and the velocity v. For the "perturbed," i.e., nonintegrable nonlinear Schrödinger equation (17), one can adapt the procedure in Refs. [58–60], to find a set of equations modeling the time variation of the above integrals, i.e., in the form

$$\frac{dE}{dT} = -i\int_{-\infty}^{\infty}(\psi f^* - \psi^* f)d\xi, \quad (22)$$

$$\frac{dM}{dT} = i\int_{-\infty}^{\infty}(\psi_\xi f^* + \psi_\xi^* f)d\xi. \quad (23)$$

Combining the expressions (20)–(23), we obtain the ordinary differential equations (ODEs) for the envelope amplitude and velocity as

$$\frac{d\rho}{dT} = -\frac{4}{3}D\rho^3, \qquad \frac{dv}{dT} = 0. \quad (24)$$

The velocity of the envelope turns out to be constant, in agreement with Ref. [3]. To trace the decay (damping) effect of the wave amplitude, we integrate Eq. (24a) and obtain an analytical expression for the wave envelope (amplitude) as follows:

$$\rho(T) = \left(\frac{8}{3}\,D\,T + \frac{1}{\rho_0^2}\right)^{-1/2}, \quad (25)$$

where ρ_0 is the initial amplitude of the electric potential (i.e., the amplitude at time $T = 0$). In the limit $T \gg 1$ (or $D \gg 1$), one is led to $\rho \simeq \sqrt{\frac{3}{8D}\frac{1}{T}}$, suggesting a decay as $\rho \sim 1/\sqrt{T}$. On the other hand, for $T \ll 1$ (or $D \ll 1$), the envelope amplitude becomes $\rho = \rho_0(1 - \frac{4}{3}D\,T\,\rho_0^2)$, suggesting that, for a negligibly small value of D, the amplitude remains approximately equal to its initial amplitude. We may now recover the dimensions of Eq. (25), in terms of the scaling in (14), for transparency; we thus obtain

$$\psi_m(\tau) = \psi_{\max}\left(\tfrac{8}{3}\,|Q_i|\,\tau\,\psi_{\max}^2 + 1\right)^{-1/2}, \quad (26)$$

where $\psi_m(\tau) = \psi_0\rho(T)$, $\tau = T/\psi_0^2|Q_r|$, and $\psi_{\max} = \psi_0\rho_0$.

V. PARAMETRIC INVESTIGATION

In order to characterize the dynamics and propagation characteristics of electron-acoustic envelope modes, we will now focus our attention on the role of dissipation (an element absent in earlier works on EAWs [41]), i.e., manifested as damping of the envelope (wave packet amplitude), and on its parametric dependence on various plasma (configuration) parameters in particular, namely the superthermality index κ, the carrier wave number k, the cold-to-hot electron density ratio β. The bright envelope soliton solution given in Eq. (20) will be considered as the initial condition.

Recall that the dispersion coefficient P is a real-valued quantity; that is, there is no gain term provided by the dispersion. On the other hand, the nonlinear coefficient Q is a complex quantity—suggesting wave propagation may be subject to the simultaneous effect of mechanisms like nonlinear wave steepening and also amplitude growth, e.g., through modulational instability (arising due to the real part of Q) [41], and energy loss (given by the imaginary part). The dispersive term may balance the nonlinear steepening term. However, as there is no external energy source to counteract (or balance) the nonlinear loss term, the wave packet is expected to suffer damping (amplitude decay) while propagating. Analytically speaking, the damping (dissipative) effect is measured by the parameter D, appearing in Eq. (17) above. The effect

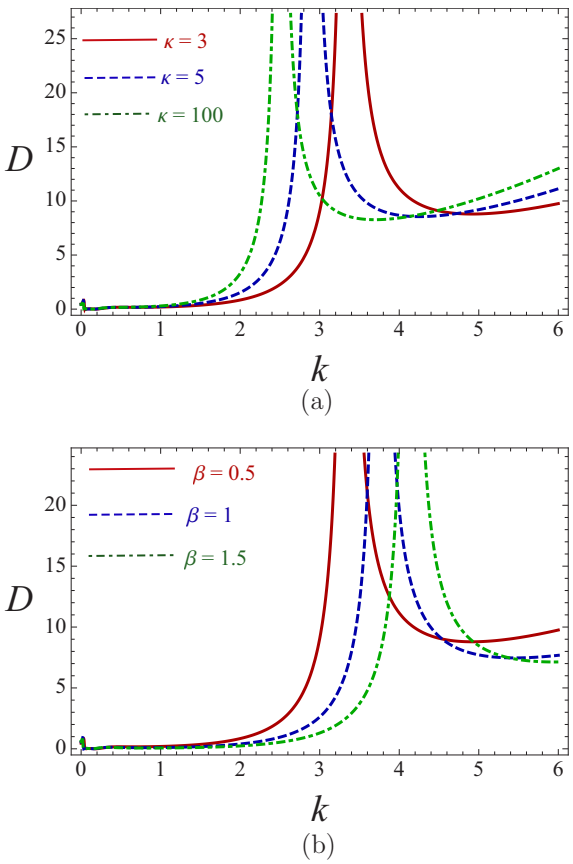

FIG. 7. The damping factor D, given in Eq. (17), is depicted versus the wave number k (a) for different superthermality κ for $\beta = 0.5$, $\nu = 0.05$, and (b) for different cold-to-hot electron density ratio β for $\kappa = 3$, $\nu = 0.05$.

of damping on the high-frequency electron-acoustic wave packets' amplitude is investigated, both analytically—based on the result given in Eq. (25) above—and numerically, for different plasma configuration parameters.

A. Analytical prediction

In Fig. 7, we show the variation of the damping factor D [given in Eq. (17)] versus the wave number for different values of (the spectral index) κ and (the cold-to-hot electron number density ratio) β. It is necessary to recall here that the dispersive term P and the imaginary part of the nonlinear term Q_i are always negative for all k, while the real part of the nonlinear term Q_r can be negative or positive depending on the plasma parameters; see Fig. 5. According to the standard theory of envelope solitons, formed by self-modulational processes—see, e.g., in Refs. [1,41,57]—envelope modes may be either of the bright (envelope pulses) or dark (envelope holes) type, depending only on the sign of the real nonlinear term Q_r, in our case [40,57]: bright solutions are obtained for $Q_r < 0$, while dark types solutions are possible for $Q_r > 0$. Now, regarding the role of dissipation, note the appearance of a vertical asymptote in the graph of $D = |Q_i/Q_r|$, corresponding to the roots of Q_r; see Fig. 7. In fact, the left three curves (preceding the asymptote) in Fig. 7 are for $Q_r > 0$ (defocusing regime, hence dark envelope soliton solutions), while the right three (i.e., for large k, following the asymptote) are for $Q_r < 0$ (focusing regime, hence bright-type soliton solutions, or breathers). Stable bright envelope modes (breathers) will therefore exist in the short-wavelength regime, while dark-type envelope solitons will be encountered for long carrier wavelengths.

The damping factor D, for given wave number k and β, is higher (suggesting stronger damping) for non-Maxwellian plasma (i.e., for smaller κ values) in the focusing region, i.e., slightly above the asymptote; see Fig. 7(a). Reversely, it appears to be lower (i.e., weaker damping) in the defocusing region, i.e., below the asymptote in Fig. 7(a). Furthermore, a qualitative effect of κ is witnessed in Fig. 7(a) (and also in Fig. 5 above), in the sense that certain wave number values may lie in the defocusing (modulationally stable) region, in the Maxwellian case (infinite κ), and still be destabilized for finite κ, entering the focusing (modulationally unstable) region. It would be interesting to consider this mechanism in realistic (e.g., space plasma) observations of electrostatic wave packets.

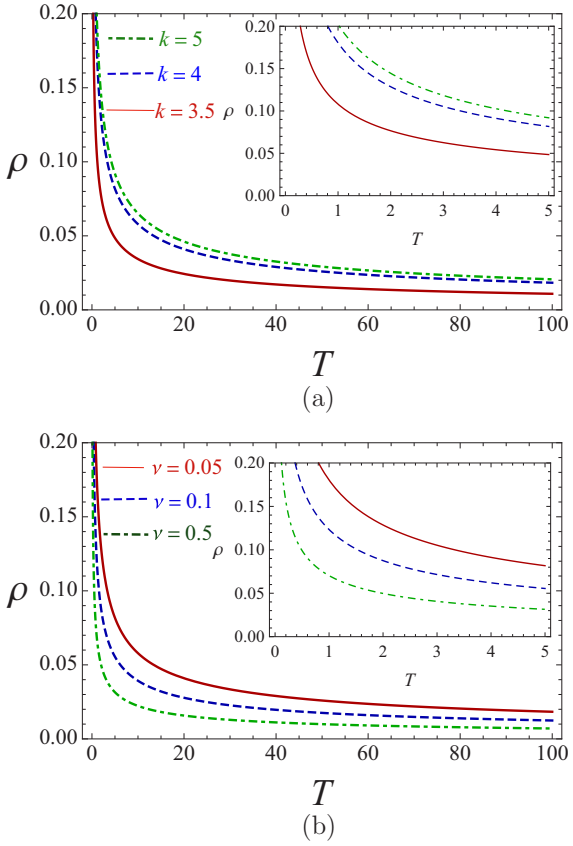

FIG. 8. The evolution of the normalized envelope amplitude ρ (in units of electric potential), as given in Eq. (25), is depicted versus time T (in units of ω_{ph}^{-1}). We have considered different values of (a) the carrier wave number k (in units of λ_{Dh}^{-1}), for collision frequency $\nu = 0.05$, and (b) the dissipation factor ν for $k = 4$. The other parameters are fixed at $\kappa = 3$, $\beta = 0.5$. The inset plots show a zoom-in view of regions of interest.

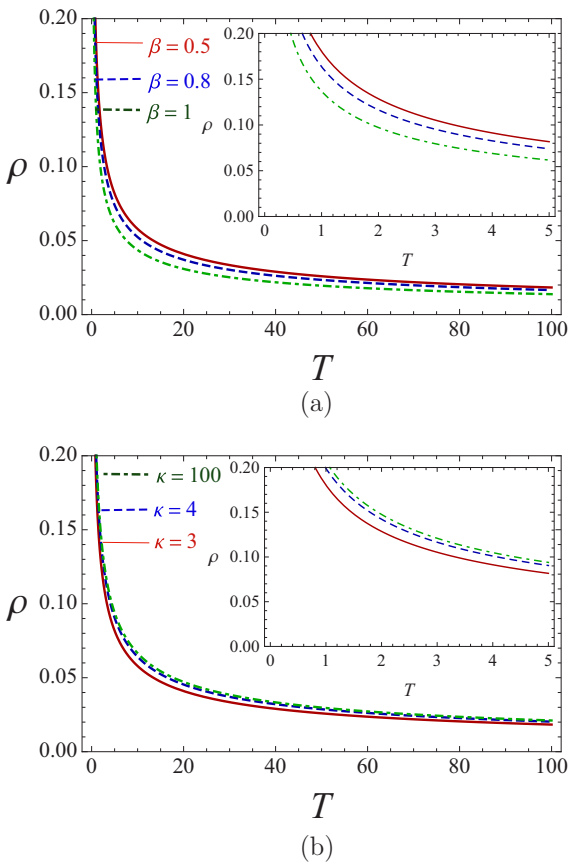

FIG. 9. The evolution of the normalized envelope amplitude ρ (in units of electric potential), as given in Eq. (25), is depicted versus time T (in units of ω_{ph}^{-1}). We have considered different values of (a) β for $\kappa = 3$, and (b) κ for $\beta = 0.5$. The other parameters are fixed at $k = 4$, $\nu = 0.05$. The inset plots show a zoom-in view of regions of interest.

In an analogous manner, some qualitative conclusions may be drawn from Fig. 7(b), regarding the damping of envelope modes and how these depend on the value of β (i.e., for given κ). Remarkably, a change of regime (from/to focusing to/from defocusing) occurs upon a continuous variation of the value of β, suggesting that the electron component configuration may act as order parameter, as regards not only envelope structures and their stability [41], but also the decay rate of the modulated envelope. The effects of the wave number and of the collisional frequency on the envelope amplitude are depicted in Fig. 8.

The effects of the cold electron concentration (via β) and of the spectral (superthermality) index κ on the envelope amplitude are shown in Fig. 9. An increase in the number density of the inertial (cold electron) component (i.e., higher β) apparently results in an increase in the collision rate in the plasma, hence higher damping; see Fig. 9(a). In a similar manner, lower κ, i.e., stronger deviation from Maxwellian equilibrium, leads to stronger damping as well, due to the increase in energetic electrons (in the hot electron component); see Fig. 9(b).

B. Numerical simulation

Our numerical analysis is based on a numerical integration of the nonlinear Schrödinger equation given in Eq. (17), by adopting a Runge-Kutta 4 (RK4) method. The time interval and the spatial grid size are taken as 2×10^{-4} and 0.015, respectively. The envelope soliton solution (20) is considered as initial condition.

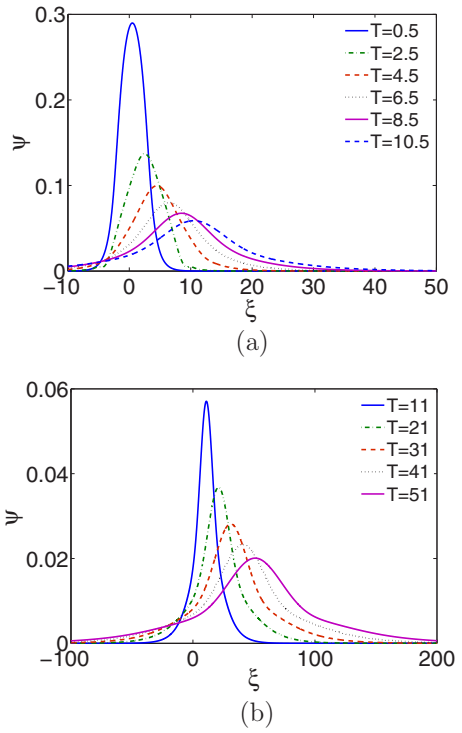

FIG. 10. The evolution in time of the (normalized) bright envelope amplitude, given by (20), is depicted. For the initial condition, based on Eq. (20), we have considered a set of representative parameter values: $k = 4$, $\kappa = 3$, $\beta = 0.5$, and $\nu = 0.05$ (implying $P = -0.0054$, $Q_r = -5.99$, and $Q_i = -66.78$). The wave amplitude ψ is shown versus position ξ, in two successive time intervals.

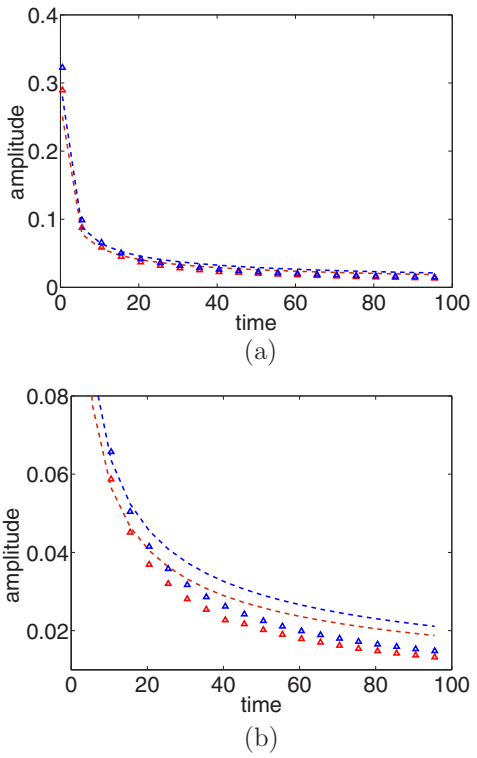

FIG. 11. The decay of the envelope soliton (pulse) amplitude with time is illustrated, as observed numerically (rectangles) and analytically (dashed line). Different values of the wave number k are considered: the red (lower) curve is for wave number $k = 4$, while the blue (upper) curve is for $k = 5$. The other parameters are taken as $\kappa = 3$, $\beta = 0.5$, and $\nu = 0.05$. A zoom-in aspect is shown in the panel (b).

Figure 10 shows the evolution of the envelope, for an *ad hoc* choice of parameter values: wave number $k = 4$, $\kappa = 3$ (relatively strong deviation from Maxwellian, a typical value in space observations [38,51]), $\beta = 0.5$ (i.e., 33% of the electrons are in the cold inertial population), and $\nu = 0.05$ (moderate damping), entailing the values $P = -0.0054$, $Q_r = -5.99$, $Q_i = -66.78$, and thus $D = 11.15$. Note that these values correspond to the focusing regime ($PQ_r > 0$). The evolution of the wave amplitude ψ (in terms of the electrostatic potential) versus position ξ, for various time instants T is depicted in Fig. 10. We notice a decaying amplitude, as time progresses, as expected, both intuitively and based on the previously obtained analytical result. A similar trend was observed for various other combinations of plasma parameter values.

Overall, we have established a dynamical system depending on various parameters (namely, k, κ, β, and ν). We have undertaken a meticulous parametric analysis, based on a series of computer simulations, varying each of these parameters independently while assuming fixed values for the remaining parameters. Our results are discussed in the following.

The dependence of amplitude decay for two different values of the carrier wave number k is considered in Fig. 11, for $\kappa = 3$, $\beta = 0.5$, and $\nu = 0.05$.

In Fig. 12, we have depicted the time-dependent (decaying) envelope, for different values of the cold-to-hot electron

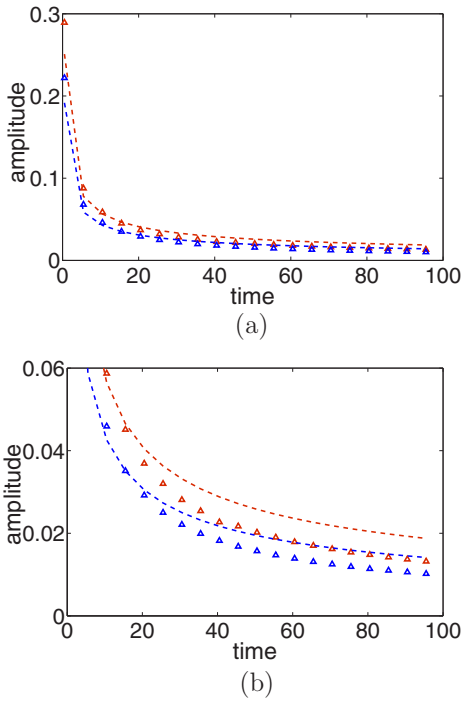

FIG. 12. The decay of the envelope soliton (pulse) amplitude with time is illustrated, as observed numerically (rectangles) and analytically (dashed line). Different values of the cold-to-hot electron density ratio β are considered: the red (upper) curve is for $\beta = 0.5$, while the blue (lower) curve is for $\beta = 1$. The other parameters are taken as $k = 4$, $\kappa = 3$, and $\nu = 0.05$. A zoom-in aspect is shown in panel (b).

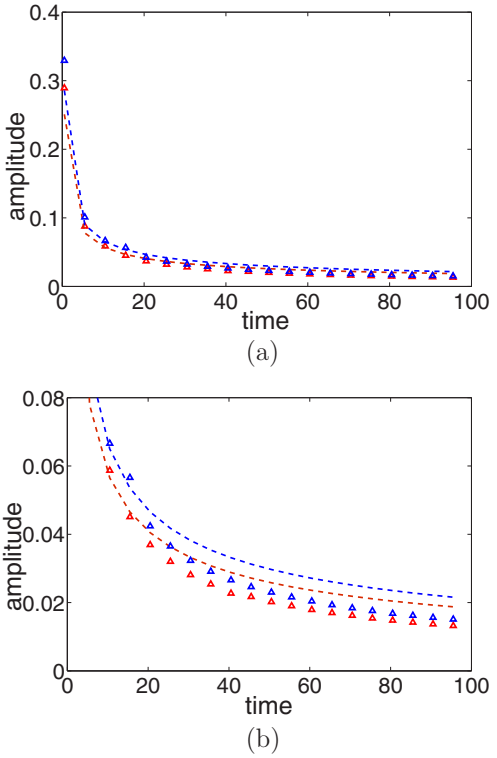

FIG. 13. The decay of the envelope soliton (pulse) amplitude with time is illustrated, as observed numerically (rectangles) and analytically (dashed line). The red (lower) curve is for $\kappa = 3$ and the blue (upper) curve is for $\kappa = 100$ (quasi-Maxwellian). The other parameters are $k = 4$, $\beta = 0.5$, and $\nu = 0.05$. A zoom-in aspect is shown in panel (b).

density ratio β, taking $\kappa = 3$, $k = 4$, and $\nu = 0.05$. We see that the damping is stronger for higher β, i.e., for a dominant cool electron population.

Finally, a strongly non-Maxwellian plasma ($\kappa = 3$) has been considered in Fig. 9(b), in comparison with a quasi-Maxwellian plasma (for $\kappa = 100$). As seen in Fig. 13, wave packets propagating in non-Maxwellian plasma suffer envelope decay at a faster pace, compared with Maxwellian plasma, in agreement with our analytical prediction in Fig. 9(b).

In all of the case considered above, the analytical and numerical results exhibit the same qualitative trend, i.e., a decaying envelope in time; however, from a quantitative point of view, the analysis—based on Eq. (25)—predicts a slower decay rate than the one observed in the computer simulation. This apparent discrepancy may arguably be attributed to the fact that the analytical prediction was obtained by assuming weak dissipation, viz., a small right-hand side of Eq. (17) above. However, in our physical system, the value of the dimensionless parameter $D = |Q_i/Q_r|$ turned out to be significant, as obvious from Fig. 7, thus partially invalidating the perturbative analysis adopted.

VI. CONCLUSION

In this paper, we have investigated the characteristics of high-frequency dissipative electron-acoustic envelope solitons in a three-component unmagnetized collisional plasma containing inertial cold electrons, inertialess nonthermal κ-distributed hot electrons, and stationary ions. Electron-neutral collisions have been taken into account, in fact held responsible for wave dissipation (damping).

A cubic NLSE with real dispersive coefficient and complex nonlinear coefficient was derived, by adopting a multiscale perturbation technique, to model the evolution of the dissipative wave packet envelope. The dispersive coefficient and the imaginary part of the nonlinear coefficient were found to be negative for all plasma parameters, while the real part of the nonlinear term is positive for long wavelengths (prescribing modulational stability) and changes sign at a certain wave number threshold (which depends on plasma configuration parameters). In our analysis, we have focused particularly on the time-dependent amplitude and velocity of the envelope solitons in order to trace the effect of dissipation.

Our results are summarized as follows:

(1) Electron-acoustic wave packets are overdamped in the long-wavelength regime; in other words, EAW propagation is not possible for small values of the carrier wave number, i.e., below a certain threshold (critical value) k_c, which increases with collisionality.

(2) The wave number threshold k_c is reduced for stronger deviation from the Maxwellian distribution for the electrons, i.e., for smaller κ, and is also reduced for higher cold electron concentration (i.e., higher value of β).

(3) The dispersive term decreases in magnitude, while the nonlinearity terms (both real and imaginary parts) increase, as κ decreases (stronger deviation from the Maxwellian equilibrium for the hot electrons).

(4) The decay rate of the envelope is higher in non-Maxwellian plasma, and also higher for stronger cold electron presence in the plasma.

(5) Approximate analysis, based on known methodology for near-integrable systems, leads to an analytical prediction for the decaying envelope that is characterized by constant velocity, and an amplitude that decays in time.

(6) A series of numerical simulations has been performed to test our analytical predictions for the envelope amplitude. The numerical outcome confirms our analytical result qualitatively and, to a satisfactory extent, also quantitatively.

Our investigation should be useful for better understanding the characteristics of modulated high-frequency electrostatic wave packets that are ubiquitous in laboratory as well as space plasmas, where a coexistence of different electron populations (at distinct temperature) occurs, in combination with weak collisionality and in the presence of energetic (suprathermal) electrons.

ACKNOWLEDGMENT

S.S. thanks the Alexander von Humboldt Foundation, Germany for financial support via a postdoctoral fellowship.

APPENDIX A: MULTIPLE SCALES PERTURBATION TECHNIQUE

The nonlinear Schrödinger equation is obtained by adopting the multiple space and time scale(s) technique [1,40,41,57], applied to Eqs. (1)–(3). The dependent variables n, u, and ϕ [let us say, the state vector $S^{(n)} = (n, u, \phi)^T$] are assumed as $S = S^{(0)} + \epsilon S^{(1)} + \epsilon^2 S^{(2)} + \cdots = S^{(0)} + \Sigma_{n=1}^{\infty} \epsilon^n S^{(n)}$, where $S^{(0)} = (1, 0, 0)^T$ is the equilibrium state vector and $\Sigma_{n=1}^{\infty} \epsilon^n S^{(n)}$ is the perturbed state with $\epsilon \ll 1$. We assume the following stretching of the space and the time coordinates: $X_n = \epsilon^n x$ and $T_n = \epsilon^n t$, respectively, where $n = 1, 2, 3, \ldots$ (viz., $X_1 = \epsilon x$, $X_2 = \epsilon^2 x$, and so forth; same for time), to be distinguished from the (*fast*) carrier variables x ($\equiv X_0$) and t ($\equiv T_0$). The slow scales, which are assumed to vary very slowly, enter the argument of the lth harmonic amplitude $S_l^{(n)}$, thus $S^{(n)} = \sum_{l=-n}^{n} S_l^{(n)}(X_j, T_j) e^{il(kx-\omega t)}$. We now substitute these assumptions into our model equations (1)–(3) and isolate the equations for different n and l.

1. Linear part

In order to get the linear set of equations, we linearize Eqs. (1)–(3), i.e., isolating the equations for $n = 1, l = 1$, and obtain

$$\begin{aligned} -i\omega n_1^{(1)} + iku_1^{(1)} &= 0, \\ -(i\omega - \nu)u_1^{(1)} - ik\phi_1^{(1)} &= 0, \\ -\beta n_1^{(1)} - (k^2 + c_1)\phi_1^{(1)} &= 0. \end{aligned}$$

That is, the compatibility condition for $n = 1$, $l = 1$ provides a dispersion relation for the electron-acoustic excitation given in Eq. (8). We also determine the first harmonic amplitudes of the perturbation from the three equations above in terms of the first-order electrostatic potential correction $\phi_1^{(1)}$ as

$$n_1^{(1)} \equiv C_1^{11}\phi_1^{(1)}, \qquad u_1^{(1)} \equiv C_2^{11}\phi_1^{(1)}, \tag{A1}$$

where the coefficients $C_j^{(11)}$ ($j = 1, 2$) are as follows:

$$\begin{aligned} C_1^{11} &= -\frac{k^2}{\omega(\omega + i\nu)} = -\frac{k^2 + c_1}{\beta}, \\ C_2^{11} &= -\frac{\omega}{k}\frac{k^2 + c_1}{\beta}. \end{aligned}$$

2. Nonlinear part

The next order perturbations, i.e., for $n = 2, l = 1$, provide the compatibility condition in the form

$$\frac{\partial \phi_1^{(1)}}{\partial T_1} + v_g \frac{\partial \phi_1^{(1)}}{\partial X_1} = 0, \tag{A2}$$

where the group velocity v_g defined as

$$v_g = \frac{d\omega}{dk} = \frac{\beta k c_1}{(k^2 + c_1)^2}\frac{2}{i\nu + 2\omega} = \frac{\omega^2(\omega + i\nu)^2}{\omega + i\nu/2}\frac{c_1}{\beta k^3} \tag{A3}$$

is a real-valued ν-dependent parameter.

a. Second-order first harmonics

The amplitudes corresponding to the first harmonics in order ϵ^2 are given by

$$\begin{aligned} n_1^{(2)} &= \frac{2ik}{\beta}\frac{\partial \phi_1^{(1)}}{\partial X_1}, \\ u_1^{(2)} &= \left[\frac{2i\omega}{\beta} + \frac{ic_1}{(k^2 + c_1)}\frac{2}{2\omega + i\nu} - \frac{i\omega}{\omega(\omega + i\nu)}\right]\frac{\partial \phi_1^{(1)}}{\partial X_1}. \end{aligned}$$

b. Second-order second harmonics

For $n = 2$ and $l = 2$, the evolution equation provides the amplitudes of the second-order second harmonic which are found to be proportional to $(\phi_1^{(1)})^2$. The expression for these amplitudes are

$$\begin{aligned} n_2^{(2)} &= C_1^{(22)}\left(\phi_1^{(1)}\right)^2 = \left[\mathrm{Re}C_1^{(22)} + i\mathrm{Im}C_1^{(22)}\right]\left(\phi_1^{(1)}\right)^2, \\ u_2^{(2)} &= C_2^{(22)}\left(\phi_1^{(1)}\right)^2 = \left[\mathrm{Re}C_2^{(22)} + i\mathrm{Im}C_2^{(22)}\right]\left(\phi_1^{(1)}\right)^2, \\ \phi_2^{(2)} &= C_3^{(22)}\left(\phi_1^{(1)}\right)^2 = \left[\mathrm{Re}C_3^{(22)} + i\mathrm{Im}C_3^{(22)}\right]\left(\phi_1^{(1)}\right)^2, \end{aligned}$$

where

$$\mathrm{Re}C_1^{(22)} = -\frac{(4k^2+c_1)}{\beta}\mathrm{Re}C_3^{(22)} - \frac{c_2}{\beta}, \qquad \mathrm{Re}C_2^{(22)} = -\frac{(k^2+c_1)^2\left(\frac{\beta k^2}{k^2+c_1} - \frac{\nu^2}{2}\right)}{2\beta^2 k(\omega + i\nu/2)} - \frac{k}{\omega + i\nu/2}\mathrm{Re}C_3^{22},$$

$$\mathrm{Re}C_3^{(22)} = \frac{12\beta k^4[-3(k^2+c_1)^2 - 2\beta c_2]}{2\beta[36\beta k^6 + \nu^2(c_1-2k^2)(k^2+c_1)(4k^2+c_1)]} + \frac{\nu^2(k^2+c_1)[-(c_1-8k^2)(k^2+c_1)^2 + 6k^2\beta c_2]}{2\beta[36\beta k^6 + \nu^2(c_1-2k^2)(k^2+c_1)(4k^2+c_1)]},$$

$$\mathrm{Im}C_1^{(22)} = -\frac{(4k^2+c_1)}{\beta}\mathrm{Im}C_3^{(22)}, \qquad \mathrm{Im}C_2^{(22)} = \mathrm{Im}C_3^{(22)} - \frac{\nu}{2}\frac{(k^2+c_1)^2}{\beta^2 k},$$

$$\mathrm{Im}C_3^{(22)} = \frac{\nu(k^2+c_1)^2\sqrt{\frac{4\beta k^2}{k^2+c_1} - \nu^2}[-3c_1(k^2+c_1) - 2\beta c_2]}{2\beta[36\beta k^6 + \nu^2(c_1-2k^2)(k^2+c_1)(4k^2+c_1)]}.$$

c. Second-order zeroth harmonics

The second-order zeroth harmonic amplitudes can be obtained by combining expressions for $n = 2, l = 0$ and $n = 3, l = 0$, and take the general form as

$$n_0^{(2)} = C_1^{(20)}|\phi_1^{(1)}|^2, \quad u_0^{(2)} = C_2^{(20)}|\phi_1^{(1)}|^2, \quad \phi_0^{(2)} = C_3^{(20)}|\phi_1^{(1)}|^2,$$

where

$$C_1^{(20)} = -\frac{1}{\beta}\left(2c_2 + c_1 C_3^{(20)}\right), \quad C_2^{(20)} = \frac{1}{v_g}\left(\frac{k^2+c_1}{\beta} - C_3^{(20)}\right),$$

$$C_3^{(20)} = \frac{1}{\beta - v_g^2 c_1}\left[2\,v_g^2 c_2 + (k^2+c_1) + \frac{2\,v_g\beta k^3(\omega + i\nu/2)}{\omega^2(\omega+i\nu)^2}\right].$$

APPENDIX B: COEFFICIENTS OF THE DISSIPATIVE NLS EQUATION

The dissipative NLS equation (14) involves the coefficients P and Q. The group velocity dispersion coefficient P $(= \frac{1}{2}\frac{d^2\omega}{dk^2})$ is a real-valued parameter, given by the expression

$$P(k,\kappa,\beta,\nu) = -\frac{\beta c_1[12k^4\beta + (c_1 - 3k^2)(k^2+c_1)\nu^2]}{(k^2+c_1)^4(2\omega + i\nu)^3}. \tag{B1}$$

The nonlinearity coefficient Q can be expressed in the form

$$Q(k,\kappa,\beta,\nu) = -\frac{\omega(\omega+i\nu)}{2\omega+i\nu}\left(C_1^{(20)} + C_1^{(22)}\right) + \frac{\nu^2}{2(2\omega+i\nu)}C_1^{(22)} - \frac{i\nu}{2}C_1^{(22)}$$
$$+\frac{\omega^2(\omega+i\nu)^2}{\beta k^2(2\omega+i\nu)}\left[2c_2\left(C_3^{(20)} + C_3^{(22)}\right) + 3c_3\right] - k\left(C_2^{(22)} + C_2^{(20)}\right) - \frac{i\nu k}{2\omega+i\nu}C_2^{(22)}, \tag{B2}$$

where all quantities are defined in the previous appendix.

Q can be expressed as $Q = Q_r + i\,Q_i$. Closed analytical expressions for the real part Q_r and the imaginary part Q_i can be explicitly obtained, in the form

$$Q_r(k,\kappa,\beta,\nu) = -\frac{\omega(\omega+i\nu)}{2\omega+i\nu}\left(C_1^{(20)} + \mathrm{Re}C_1^{(22)}\right) + \frac{\nu^2}{2(2\omega+i\nu)}\mathrm{Re}C_1^{(22)} + \frac{\nu}{2}\mathrm{Im}C_1^{(22)}$$
$$+\frac{\omega^2(\omega+i\nu)^2}{\beta k^2(2\omega+i\nu)}\left[2c_2\left(C_3^{(20)} + \mathrm{Re}C_3^{(22)}\right) + 3c_3\right] - k\left(\mathrm{Re}C_2^{(22)} + C_2^{(20)}\right) + \frac{\nu k}{2\omega+i\nu}\mathrm{Im}C_2^{(22)}, \tag{B3}$$

$$Q_i(k,\kappa,\beta,\nu) = -\frac{\omega(\omega+i\nu)}{2\omega+i\nu}\mathrm{Im}C_1^{(22)} + \frac{\nu^2}{2(2\omega+i\nu)}\mathrm{Im}C_1^{(22)} - \frac{\nu}{2}\mathrm{Re}C_1^{(22)} - k\mathrm{Im}C_2^{(22)} - \frac{\nu k}{2\omega+i\nu}\mathrm{Re}C_2^{(22)}$$
$$+\frac{\omega^2(\omega+i\nu)^2}{\beta k^2(2\omega+i\nu)}2c_2\mathrm{Im}C_3^{(22)}. \tag{B4}$$

The various quantities in the latter expressions are given in Appendix A.

APPENDIX C: APPROXIMATE EXPRESSIONS FOR SMALL ν

The dispersion term, given in Eq. (B1), can be expressed as

$$P(k,\kappa,\beta,\nu) = p_0 + p_1\,\nu^2 + \cdots, \tag{C1}$$

where

$$p_0 = -\frac{3\left(\kappa - \frac{1}{2}\right)\sqrt{\frac{\beta k^2}{\frac{2}{2\kappa-3}+k^2+1}}}{2\left(\kappa - \frac{3}{2}\right)\left(\frac{2}{2\kappa-3}+k^2+1\right)^2} \tag{C2}$$

and

$$p_1 = -\frac{(2\kappa-1)[4\kappa+(6\kappa-9)k^2-2]}{16k^2[2\kappa+(2\kappa-3)k^2-1]^2\sqrt{\frac{\beta(2\kappa-3)k^2}{2\kappa+(2\kappa-3)k^2-1}}}. \tag{C3}$$

It is obvious and also justified from our plasma model that p_0 is exactly the same as the dispersion coefficient in Ref. [40] in the absence of collisional damping ν. Approximate values of p_0 and p_1 for the Maxwellian case can be recovered for the limit $\kappa \to \infty$, which read

$$p_{0\mathrm{Max}} = -\frac{3\sqrt{\beta}k}{2(k^2+1)^{5/2}}, \tag{C4}$$

$$p_{1\mathrm{Max}} = \frac{-3k^2-2}{16\sqrt{\beta}k^3(k^2+1)^{3/2}}, \tag{C5}$$

where $p_{0\mathrm{Max}}$ refers to the dispersion coefficient for EAWs in Maxwellian plasmas in the absence of collisional effect and matches with the dispersion term in Ref. [41]. Similarly, the real nonlinear term Q_r and the imaginary nonlinear term Q_i can be written as

$$Q_r = q_{r0} + q_{r1}\,\nu^2 + \cdots, \quad Q_i = q_{i1}\,\nu + q_{i2}\,\nu^3 + \cdots, \tag{C6}$$

where expressions of q_{r0}, q_{r1}, q_{i1}, q_{i2}, are very long and omitted here. q_{r0} represents the nonlinear term for $\nu = 0$ as in Ref. [40], and one can easily recover the Maxwellian case for collisionless plasma [41] by considering the limit $\kappa \to \infty$ and $\nu = 0$.

[1] T. Dauxois and M. Peyrard, *Physics of Solitons* (Cambridge University Press, Cambridge, 2006).
[2] Y. S. Kivshar and B. A. Malomed, Rev. Mod. Phys. **61**, 763 (1989).
[3] D. R. Nicholson and M. V. Goldman, Phys. Fluids. **19**, 1621 (1976).
[4] N. R. Pereira and L. Stenflo, Phys. Fluids. **20**, 1733 (1977).
[5] N. R. Pereira, Phys. Fluids. **20**, 1735 (1977).
[6] N. R. Pereira and Flora Y. F. Chu, Phys. Fluids. **22**, 874 (1978).
[7] S. Sultana and I. Kourakis, in *Proceedings of the 37th EPS Conference, Dublin, Ireland, 21–25 June 2010*, Europhysics Conference Abstracts, Vol. 34A (2010), paper P2.411; available at http://ocs.ciemat.es/EPS2010PAP/pdf/P2.411.pdf.
[8] M. Dutta, S. Ghosh, and N. Chakrabarti, Phys. Rev. E **86**, 066408 (2012).
[9] S. Ghosh, A. Adak, and M. Khan, Phys. Plasmas **21**, 012303 (2014).
[10] S. Sultana and I. Kouraki, Phys. Plasmas **22**, 102302 (2015).
[11] L. F. Mollenauer, R. H. Stolen, and J. P. Gordon, Phys. Rev. Lett. **45**, 1095 (1980).
[12] K. Nozaki and N. Bekki, Phys. Rev. Lett. **51**, 2171 (1983).
[13] V. V. Afanasjev, Opt. Lett. **20**, 704 (1995).
[14] B. A. Malomed and H. G. Winful, Phys. Rev. E **53**, 5365 (1996).
[15] J. Atai and B. A. Malomed, Phys. Rev. E **54**, 4371 (1996).
[16] J. M. Soto-Crespo, N. N. Akhmediev, V. V. Afanasjev, and S. Wabnitz, Phys. Rev. E **55**, 4783 (1997).
[17] S. A. Khrapak and G. Morfill, Phys. Plasmas **8**, 2629 (2001).
[18] S. V. Vladimirov, K. N. Ostrikov, and M. Y. Yu, Phys. Rev. E **60**, 3257 (1999).
[19] R. P. H. Chang and M. Porkolab, Phys. Rev. Lett. **25**, 1262 (1970).
[20] V. Nosenko and J. Goree, Phys. Rev. Lett. **93**, 155004 (2004).
[21] V. M. Vasyliunas, J. Geophys. Res. **73**, 2839 (1968).
[22] C. Vocks, G. Mann, and G. Rausche, Astron. Astrophys. **480**, 527 (2008).
[23] C. Vocks and G. Mann, Astrophys. J. **593**, 1134 (2003).
[24] G. Gloeckler and L. A. Fisk, Astrophys. J. **648**, L63 (2006).
[25] M. A. Hellberg, R. L. Mace, T. K. Baluku, I. Kourakis, and N. S. Saini, Phys. Plasmas **16**, 094701 (2009).
[26] M. Maksimovic, V. Pierrard, and J. F. Lemaire, Astron. Astrophys. **324**, 725 (1997).
[27] C. C. Chaston, Y. D. Hu, and B. J. Fraser, Geophys. Res. Lett. **24**, 2913 (1997).
[28] G. Livadiotis and D. J. McComas, Space Sci. Rev. **175**, 183 (2013).
[29] G. Livadiotis (ed.), *Kappa Distributions: Theory and Applications in Plasmas* (Elsevier, New York, 2017).
[30] M. Lazar, I. Kourakis, S. Poedts, and H. Fichtner, Planet. Space Sci. **156**, 130 (2018).
[31] H.-J. Kunze and H. R. Griem, Phys. Rev. Lett. **21**, 1048 (1968).
[32] Y. Kuramitsu, Y. Sakawa, T. Kato, H. Takabe, and M. Hoshino, Astrophys. J. Lett. **682**, L113 (2008).
[33] G. Sarri, M. E. Dieckmann, C. R. D. Brown, C. A. Cecchetti, D. J. Hoarty, S. F. James, R. Jung, I. Kourakis, H. Schamel, O. Willi, and M. Borghesi, Phys. Plasmas **17**, 010701 (2010).
[34] S. Sultana, I. Kourakis, and M. A. Hellberg, Phys. Plasmas **17**, 032310 (2010).

[35] T. K. Baluku, M. A. Hellberg, I. Kourakis, and N. S. Saini, Phys. Plasmas **17**, 053702 (2010).
[36] S. Devanandhan, S. V. Singh, and G. S. Lakhina, Phys. Scr. **84**, 025507 (2011).
[37] S. Sultana, G. Sarri, and I. Kourakis, Phys. Plasmas **19**, 012310 (2012).
[38] I. Kourakis, S. Sultana, and M. A. Hellberg, Plasma Phys. Controlled Fusion **54**, 124001 (2012).
[39] T. K. Baluku and M. A. Hellberg, Phys. Plasmas **19**, 012106 (2012).
[40] S. Sultana and I. Kourakis, Plasma Phys. Controlled Fusion **53**, 045003 (2011).
[41] I. Kourakis and P. K. Shukla, Phys. Rev. E **69**, 036411 (2004).
[42] H. A. Haus and W. S. Wong, Rev. Mod. Phys. **68**, 423 (1996).
[43] M. Nakazawa, E. Yamada, H. Kubota, and K. Suzuki, Electron. Lett. **27**, 1270 (1991).
[44] K. Watanabe and T. Taniuti, J. Phys. Soc. Jpn. **43**, 1819 (1977).
[45] M. Y. Yu and P. K. Shukla, J. Plasma Phys. **29**, 409 (1983).
[46] R. L. Tokar and S. P. Gary, Geophys. Res. Lett. **11**, 1180 (1984).
[47] S. P. Gary and R. L. Tokar, Phys. Fluids **28**, 2439 (1985).
[48] R. L. Mace and M. A. Hellberg, J. Plasma Phys. **43**, 239 (1990).
[49] T. Stix, *Waves in Plasmas* (American Institute of Physics, New York, 1992).
[50] R. A. Treumann and W. Baumjohann, *Advanced Space Plasma Physics* (Imperial College Press, London, 1997).
[51] P. Schippers *et al.*, J. Geophys. Res. **113**, A07208 (2008).
[52] R. L. Mace, S. Baboolal, R. Bharuthram, and M. A. Hellberg, J. Plasma Phys. **45**, 323 (1991).
[53] S. Sultana, I. Kourakis, and M. A. Hellberg, Plasma Phys. Controlled Fusion **54**, 105016 (2012).
[54] S. Sultana and I. Kourakis, Eur. Phys. J. D **66**, 1 (2012).
[55] T. K. Baluku and M. A. Hellberg, Phys. Plasmas **15**, 123705 (2008).
[56] R. L. Mace, G. Amery, and M. A. Hellberg, Phys. Plasmas **6**, 44 (1999).
[57] I. Kourakis and P. K. Shukla, Nonlin. Proc. Geophys. **12**, 407 (2005).
[58] A. I. Maimistov, J. Exp. Theor. Phys. **77**, 727 (1993).
[59] N. N. Akhmediev and A. Ankiewicz, *Solitons: Nonlinear Pulses and Beams* (Chapman and Hall, London, 1997).
[60] N. N. Akhmediev and A. Ankiewicz, Lect. Notes Phys. **751**, 1 (2008).
[61] R. Fedele and H. Schamel, Eur. Phys. J. B **27**, 313 (2002).
[62] R. Fedele, Phys. Scr. **65**, 502 (2002).
[63] R. Fedele, H. Schamel, and P. K. Shukla, Phys. Scr. **T98**, 18 (2002).
[64] Y. S. Kivshar and G. P. Agrawal, *Optical Solitons from Fibers to Photonics Crystals* (Academic Press, San Diego, 2003).
[65] From Eq. (4) in Ref. [56], one obtains $k^2\omega_{pc}^2\lambda_{\kappa h}^2 = k^2(\beta/c_1)v_h^2$, which leads to $\lambda_{\kappa h} = (\beta/c_1)^{1/2}(v_h/\omega_{pc}) = (\beta/c_1)^{1/2}\lambda_{Dc}$; hence, the κ-dependent screening length, normalized by λ_{Dc}, can be expressed as $(\beta/c_1)^{1/2}$, in agreement with our result.